# Analysis, design and optimization of compact ultra-high sensitivity coreless induction coil sensors

OPEN ACCESS
IOP Publishing
Measurement Science and Technology
Meas. Sci. Technol. **31** (2020) 065902 (10pp)
https://doi.org/10.1088/1361-6501/ab7166

# Analysis, design and optimization of compact ultra-high sensitivity coreless induction coil sensors

**Matthias Ratajczak and Thomas Wondrak**

Helmholtz-Zentrum Dresden - Rossendorf, Institute of Fluid Dynamics,
Bautzner Landstraße 400, 01328 Dresden, Germany

E-mail: m.ratajczak@hzdr.de

Received 8 November 2019, revised 22 January 2020
Accepted for publication 29 January 2020
Published 31 March 2020

**Abstract**

For contactless inductive flow tomography we require a compact magnetic field measurement system with a dynamic range of 5 orders of magnitude in order to detect the amplitude and the phase of an alternating magnetic field of 1 mT strength with a precision better than 5 nT and a phase error no larger than $10^{-2}$ deg. In some applications a static magnetic field of about 300 mT is also present, resulting in a total dynamic range of 7 orders of magnitude.

We present theoretical and experimental analyses of absolute and first order gradiometric induction coil sensors with sensitivities larger than 500 V/T · Hz) and diameters of 28 mm. From their equivalent circuits, we derive the associated complex-valued transfer functions and fit these to calibration measurements, thereby determining the value of the equivalent circuit components. This allows us to compensate their non-linear frequency-dependent amplitude and phase behaviour. Furthermore, we demonstrate the optimization of coils based on Brooks' design of equal squares in the adaptation by Murgatroyd, which maximizes the inductance (and thereby most likely the sensitivity) of the coils. Finally, we design a new coil with a diameter of 74 mm and a sensitivity of 577 V/(T · Hz) with an analytically predicted equivalent magnetic field noise of around 40 pT/$\sqrt{\text{Hz}}$ in the 1 Hz frequency range, which is then confirmed by measurements on the manufactured prototype.

Keywords: magnetic field measurement, induction coil, gradiometric coil, contactless inductive flow tomography

(Some figures may appear in colour only in the online journal)

## 1. Introduction

For contactless inductive flow tomography (CIFT), which is able to measure the three-dimensional flow field of liquid metals [1, 2], a magnetic field measurement system with a dynamic range of 5 orders of magnitude is needed to measure the flow-induced magnetic field changes of an applied magnetic field outside the melt. For this technique, an alternating primary magnetic field of about 1 mT permeates a flowing melt. The interaction between the primary field and the melt creates an alternating secondary magnetic field with a strength of 100 nT. The secondary magnetic field has to be extracted from the superposition of the primary and the secondary field with a precision better than 5 nT. In some cases an additional DC magnetic field with an amplitude of 300 mT can be present as well [3, 4]. The resulting total dynamic range of 7 orders of magnitude creates a huge challenge even for modern magnetic field sensors.

Furthermore we found that in these experiments magnetic field sources with frequencies similar to our excitation

frequency and varying phases are present [4]. The required extraction of the flow-induced magnetic field therefore needs to be executed with a phase error no larger than $10^{-2}$ deg.

### 1.1. Why induction coils?

Fluxgate sensors, even though they exhibit the necessary precision, are not usable here since their magnetic core saturates at roughly 1 mT. SQUIDs are generally able to cover the whole magnetic field range required here, but because their working principle is based on superconductivity they must be cooled to very low temperatures; the corresponding complexity is not desirable in our case. GMRs are ruled out as well, since their *R-H*-characteristic exhibit hysteresis effects and non-linearities up to a few percent of their maximum range [5]. At this time these effects cannot be compensated with the precision necessary for our application [6, 7].

While more novel sensors like MEMS magnetic resonators are increasing in popularity, they cannot be employed here, since their operating principle is based on Lorentz forces that arise from the interaction of an internal field source with the external field [8, 9]. This causes them to detect both DC and AC magnetic fields. Therefore, they would require to resolve the full 7 orders of magnitude of dynamic range. To our knowledge, there exists no MEMS sensor that can reliably resolve signals with such high dynamic range. For further information about other magnetic sensing techniques, refer to [10, 11].

Since induction coil sensors do not pick up constant magnetic fields and thereby reduce the dynamic range of the magnetic input signal from 7 to only 5 orders of magnitude, these are well-suited for this task.

### 1.2. Design considerations

In their most basic form, induction coils consist of a few turns of an electrical conductor positioned in a magnetic field $\vec{B}$ with the coil's cross-section oriented perpendicularly to the flux lines (see figure 1). At the terminals of the coil a voltage $U$ can be measured that is proportional to the time-derivative of the enclosed magnetic flux. This simple design comes with the advantage of perfect linearity regarding the magnetic field amplitude and a non-existent upper range limit; the lower resolution limit is determined by the noise in the coil.

In the past decades, numerous improvements to the basic principle became available, which result in four design choices for the experimentalist. The first one concerns the order of the sensor. The basic coil design from figure 1 represents an absolute induction coil sensor, since the absolute value of the time-derivative of the magnetic flux is measured. Additionally, a differential measurement of the output voltage between two or more coils (typically connected in opposing polarity) is possible, which allows determining the spatial gradient of the magnetic field. Consequently, such sensors are labeled gradiometric induction coils [12]. A gradiometric sensor consisting of two coils would be called a 1st order gradiometric sensor, three coils constitute a 2nd order gradiometric sensor, and so on.

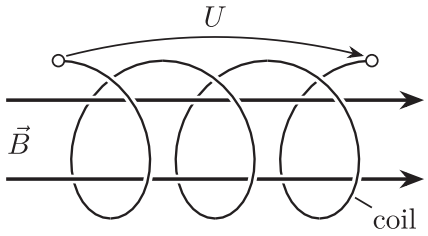


**Figure 1.** A simple cylindrical induction coil permeated by an orthogonal magnetic field.

Another possibility for optimization is the usage of ferromagnetic cores inside the windings [13] or flux concentrators in front or behind the windings [14]. Ferromagnetic materials concentrate the surrounding magnetic flux within the effective area of the sensor, thereby dramatically increasing its sensitivity and lowering the equivalent magnetic noise, which also allows for smaller sensor designs. Typically, high permeability materials like Metglas or permalloy are used for this [15], which exhibit values of $\mu_r > 90\,000$. Consequently, such coils show performance parameters similar to those of fluxgate sensors, which typically exhibit 100 pT resolution and a linearity error better than 10 ppm [16]. Albeit, induction coils with ferromagnetic components also inherit the fluxgates' disadvantage of a rather small upper range limit of about 1 mT caused by onsetting saturation effects in the ferromagnetic material.

The third design choice to make is the operation mode of the coil, which can be either voltage mode or current mode. In voltage mode, the input resistance of the attached measurement equipment has to be sufficiently large, which leads to a linear and $f$-proportional amplitude response below the resonance frequency of the coil. In comparison, in current mode the coil is operated with a shorted output, thereby circumventing the parasitic capacitance of the coil. This ultimately leads to a flat amplitude response for frequencies $f > R \cdot (2\pi L)^{-1}$ [15, 17].

Finally, the sensor design needs some kind of readout circuit. This can range from simple multimeters over analog-digital converters (ADC) to amplifiers, integrators [18], current-to-voltage converters and flux-feedback circuits [19, 20].

### 1.3. Design evaluation

In this paper, we will evaluate different sensor designs using three basic electrical performance numbers. The first one is the sensitivity of the coil, which is the ratio of output voltage per input magnetic field strength, and can be as small as 1 mV/T or as large as 1 GV/T [13, 21], especially when the size of the coil is not limited by outside factors [22], and flux concentrators and high-gain amplifiers are employed.

Secondly, the transfer function of the design plays an important role, as it determines the amplitude and phase response, both of which exhibit nonlinear frequency-dependent characteristics. The transfer function can be used advantageously, for example if the field to be measured has

a constant known frequency, the resonance frequency can be designed to match the excitation frequency, thereby increasing the effective sensitivity of the sensor. The phase response of induction coil sensor designs is often overlooked in the literature, with a few exceptions [23].

Finally, a good sensor design should minimize noise. The total voltage or current noise of the coil and the attached circuit is typically converted to equivalent input magnetic field noise, which facilitates comparing different designs. Besides using low-noise readout electronics, a coil design with minimal inherent noise is of great importance. The usage of cooling systems, e.g. with liquid nitrogen, can also greatly reduce noise [15], although this is not practical for our purposes.

Based on these deliberations we chose to solve the measurement task mentioned at the beginning of the introduction with absolute and 1st order gradiometric coreless induction coil sensors, operated in voltage mode with direct readout by a high-precision ADC. In order to measure the described minuscule magnetic fields in compact experiments, the coils need a very high turn count of about 100 000 of small-diameter wire in the order of 20 to 100 µm, with overall dimensions in the range of a few centimeters.

Such induction coils exhibit some disadvantages. Their frequency-proportional sensitivity causes increased susceptibility to high-frequency magnetic noise, which can be found in most environments. If further requirements are to be met, like increased temperature resistance, these coils can be rather expensive with costs between 200 and 500 Euro per piece. Additionally, the mass of the winding and the small wire diameter make the coils susceptible to damage through jerking motion. A broken wire inside the winding cannot be repaired, so the coils must be handled with utmost care.

### *1.4. Aims and structure*

This paper is organized as follows: To achieve the goal of minimizing amplitude and phase uncertainty, section 2 will introduce in the theory of induction coils as used for CIFT and devise their complex-valued transfer function. In section 3 the model equations will then be fitted to calibration measurements for a few frequencies. The model can then be used to calculate and correct the phase and amplitude response for any frequency.

The second goal is to design a new absolute induction coil with optimum sensitivity-to-noise ratio, which will be covered in section 4. Finally, we will focus on analytical predictions of sensor noise and confirming measurements in section 5. From this analysis, we will obtain the equivalent bandwidth-normalized input magnetic field noise, which can be used to estimate the sensors measurement uncertainty, which is the third goal of this paper.

Note that the measurement task for which all coils in this paper were designed is rather special. We are unaware of literature from other researchers where coils with similar size, turn count, sensitivity and usable frequency range are described. Therefore no comparison to similar works will be carried out in this article.

## 2. Theoretical background

Coreless induction coil sensors rely on Faraday's principle of induction, stating that a time-varying magnetic field creates an electric field in electric conductors. Let $U_{\mathrm{ind}} = U_{\mathrm{ind}}(t)$ be the induced voltage in a coil with number of turns $n$ and a cross-section of area $A$ which is permeated by a magnetic field with flux density $B$ varying over time $t$. Let furthermore the magnetic field and the cross-section be orthogonal to one another (figure 1). The basic relationship between these quantities is then

$$U_{\mathrm{ind}}(t) = -nA\frac{\partial B}{\partial t}. \tag{1}$$

In this paper we will focus on cylindrical coils with thick layers, leading to significant differences between the outer diameter $d_o$ and the inner diameter $d_i$ of the windings. In this case, the mean effective area is

$$A = \frac{1}{d_o - d_i}\int_{d_i}^{d_o}\frac{\pi}{4}y^2\mathrm{d}y = \frac{\pi}{12}\frac{d_o^3 - d_i^3}{d_o - d_i}. \tag{2}$$

If we furthermore assume $B$ to be time-harmonic

$$B(t) = -\widehat{B}\cdot\sin(2\pi f\cdot t + \varphi_0) \tag{3}$$

with amplitude $\widehat{B}$, frequency $f$ and zero-phase $\varphi_0$, we find

$$U_{\mathrm{ind}}(t) = \underbrace{nA\cdot 2\pi}_{=S}\cdot f\cdot\widehat{B}\cdot\cos(2\pi f\cdot t + \varphi_0). \tag{4}$$

The product $S$ will be labeled the sensitivity of the coil with units of $[S] = \mathrm{V}/(\mathrm{T}\cdot\mathrm{Hz})$, and is fully determined by the geometric properties of the coil.

The equivalent circuit of an absolute induction coil sensor with attached ADC is shown in figure 2(a). The coil itself comprises the equivalent source voltage $U_{\mathrm{ind}}(t)$, the series resistance $R_s$, the series inductance $L_s$ and the parasitic capacitance $C_p$. The coil is connected to an ADC with terminal resistor $R_t$ and terminal capacitance $C_t$. The voltage $U_t(t)$ is measured across the parallel circuit of $C_p$, $R_t$ and $C_t$. Instead of a time-harmonic analysis of this circuit, we analyze it in the complex domain. Therefore, the time-dependent voltages are now denoted as the complex-valued $\underline{U}_{\mathrm{ind}}$ and $\underline{U}_t$.

The relationship between the measured $\underline{U}_t$ and induced $\underline{U}_{\mathrm{ind}}$ is given by

$$\underline{U}_t(\mathrm{j}\omega) = \underline{a}_{\mathrm{abs}}(\mathrm{j}\omega)\underline{U}_{\mathrm{ind}}(\mathrm{j}\omega), \tag{5}$$

where $\underline{a}_{\mathrm{abs}}(\mathrm{j}\omega)$ is the complex-valued transfer function of the voltage divider:

$$\underline{a}_{\mathrm{abs}}(\mathrm{j}\omega) = \frac{R_t \,\|\, \frac{1}{\mathrm{j}\omega(C_p+C_t)}}{R_s + \mathrm{j}\omega L_s + \left(R_t \,\|\, \frac{1}{\mathrm{j}\omega(C_p+C_t)}\right)}. \tag{6}$$

In these equations $\omega = 2\pi f$ is the angular frequency and $\mathrm{j} = \sqrt{-1}$ the imaginary unit. The $\|$ operator denotes a parallel circuit

$$x_1 \,\|\, x_2 = \frac{x_1 x_2}{x_1 + x_2}. \tag{7}$$

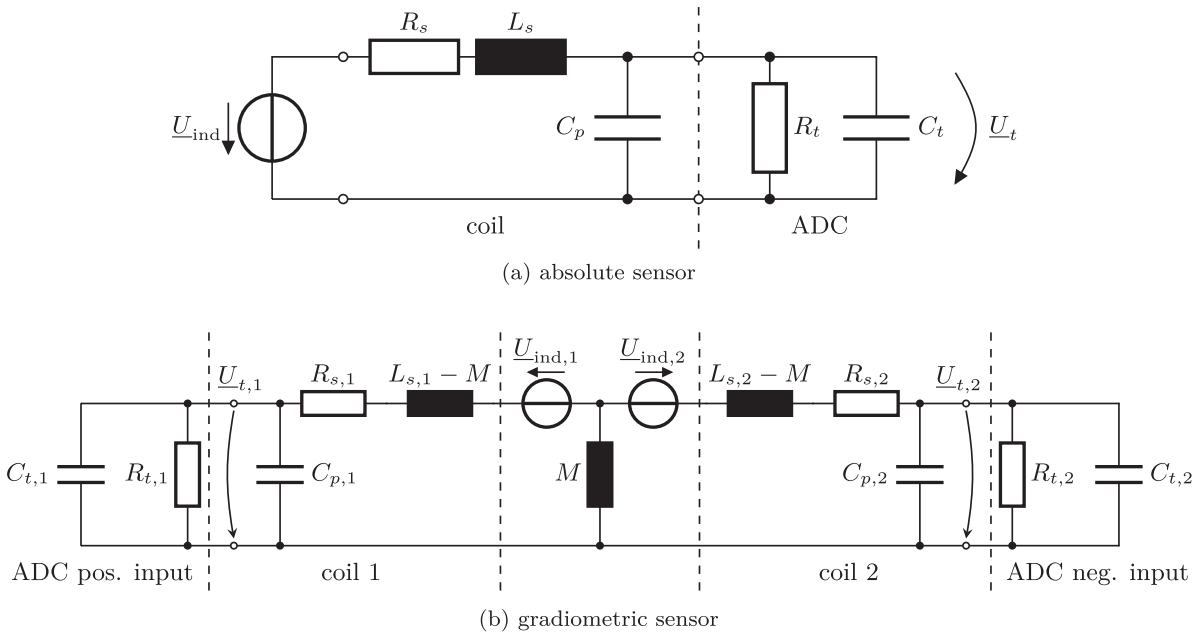


**Figure 2.** Equivalent circuit diagram of both coil types.

For a 1st order gradiometric coil, the equivalent circuit is shown in figure 2(b). It comprises two absolute coils with their individual resistance, inductance and capacitance. The readout is realized in form of the differential input of the ADC, with the right branch connected to the positive input and the left branch connected to the negative input. Both the left and right ends of the circuit are also coupled to one another by an additional parasitic capacitance not shown here since it does not have a significant effect on the transfer function in our case, as can be seen after fitting the data in the following section. Omitting the capacitance greatly facilitates the calculations for this network.

Since both individual coils are magnetically coupled, they represent a transformer. In this circuit, $M$ is the mutual inductance between both coils with

$$M = k_c\sqrt{L_{s,1}L_{s,2}} \quad \text{for } |k_c| \leq 1. \tag{8}$$

The factor $k_c$ is the coupling coefficient, which would be close to 1 for a transformer, but in our case has a smaller value because of the coreless design and the distance between the two windings. Furthermore, it is negative, since both coils are connected with opposing signs. The effective inductance of each individual coil is the so-called 'stray inductance':

$$L_\sigma = L_s - M. \tag{9}$$

The resulting electric network is evaluated by utilizing the superposition principle and calculating equivalent two-port networks. At first, we assume the two branches of the network to be symmetric:

$$\begin{aligned} R_{t,1} &= R_{t,2} = R_t, \\ R_{s,1} &= R_{s,2} = R_s, \\ L_{s,1} &= L_{s,2} = L_s, \\ C_{t,1} &= C_{t,2} = C_t, \\ C_{p,1} &= C_{p,2} = C_p. \end{aligned}$$

Afterwards the circuit can be simplified into the following impedances:

$$\underline{Z}_t = R_t \left\| \frac{1}{\mathrm{j}\omega C_t} \right\| \frac{1}{\mathrm{j}\omega C_p}, \tag{10}$$

$$\underline{Z}_s = \underline{Z}_t + R_s + \mathrm{j}\omega(L_s - M), \tag{11}$$

$$\underline{Z}_c = \underline{Z}_s \parallel \mathrm{j}\omega M, \tag{12}$$

$$\underline{Z} = \underline{Z}_s + \underline{Z}_c. \tag{13}$$

From this, the transfer functions of both branches can be written as

$$\underline{a}_{\mathrm{grad},1}(\mathrm{j}\omega) = \frac{\underline{Z}_t}{\underline{Z}_s + \underline{Z}_c}, \tag{14}$$

$$\underline{a}_{\mathrm{grad},2}(\mathrm{j}\omega) = \frac{\underline{Z}_c \cdot \underline{Z}_t}{\underline{Z} \cdot \underline{Z}_s}. \tag{15}$$

Finally, both terminal voltages can be calculated from the induced voltage in either individual coil. This allows the calculation of the differential voltage $\underline{U}_t = \underline{U}_t(\mathrm{j}\omega)$ using

$$\underline{U}_{t,1} = \underline{a}_{\mathrm{grad},1} \cdot \underline{U}_{\mathrm{ind},1} + \underline{a}_{\mathrm{grad},2} \cdot \underline{U}_{\mathrm{ind},2}, \tag{16}$$

$$\underline{U}_{t,2} = \underline{a}_{\mathrm{grad},1} \cdot \underline{U}_{\mathrm{ind},2} + \underline{a}_{\mathrm{grad},2} \cdot \underline{U}_{\mathrm{ind},1}, \tag{17}$$

$$\underline{U}_t = \underline{U}_{t,1} - \underline{U}_{t,2}. \tag{18}$$

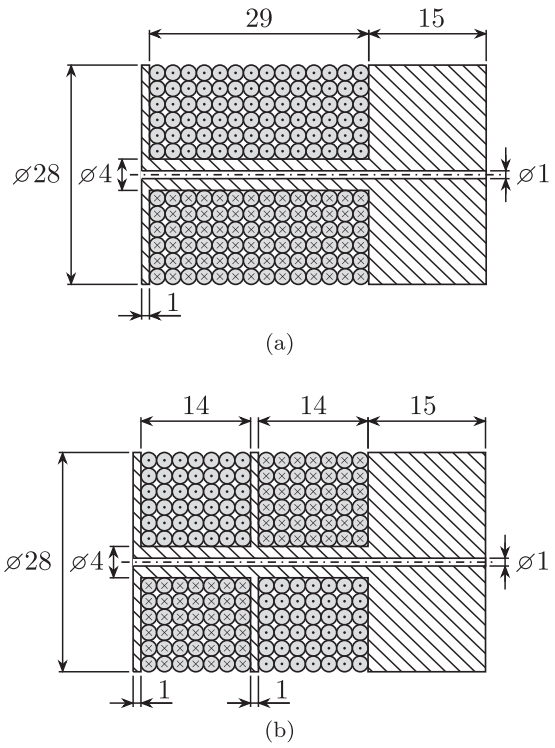


**Figure 3.** Sketch of the (a) 340k absolute and (b) 2x160k gradiometric induction coil sensor design as used for CIFT (all dimensions in mm, wire diameter not to scale)

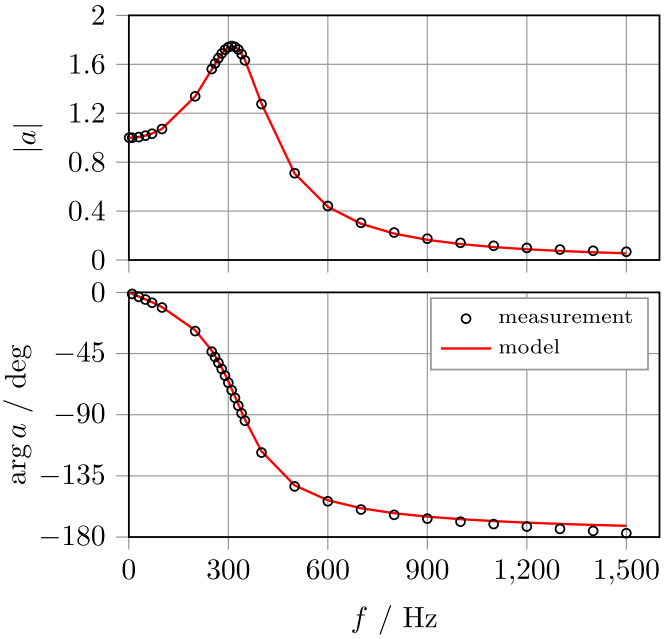


**Figure 4.** Measurement and fitted model for the 340k absolute sensor. For the sake of clarity, not all measurement points below 100 Hz are shown.

## 3. Sensor calibration

The calibration of sensor coils serves the purpose of empirically determining their sensitivity, amplitude response and phase response. We employed the calibration specifically to fit our models to the measured amplitude and phase responses for certain frequencies. The quantities $L_s$ and $C_p$ were selected as parameters for the fit. Using the fitted model, we can correct the amplitude factor and phase shift of the coils for any frequency.

For the first calibration measurements, we used available cylindrical induction coil sensors of both the absolute and 1st order gradiometric type, as can be seen in figure 3. The absolute sensor type with 340 000 turns of a 25 µm wire is labeled '340k coil', and the gradiometric sensor type with 2 times 160 000 turns of the same wire is designated '2x160k coil'. Since the signal analysis for CIFT exclusively takes place in the digital domain, we minimize the amount of analog circuitry and feed the output voltage of the coils directly into a high-precision analog-to-digital converter, in particular the model LTT24 from Labortechnik Tasler.

For the purpose of calibration we positioned one of the available absolute coils in the center of a sufficiently large Helmholtz coil pair with radius $R = 142$ mm. We then measured the amplitude and phase response of the coil in relation to the excitation current driving the magnetic Helmholtz field. When this is conducted for a sufficient numbers of frequencies (40 in our case), the models from section 2 can be fitted to the measured data, thereby obtaining the inductance and capacitance of the coil. The resistance can easily be measured with any multimeter.

Since gradiometric coils generate no output voltage for homogeneous magnetic fields, for these the Helmholtz coils are employed as Maxwell coils instead, which generate a magnetic field with nearly constant gradient in the center of both coils. For gradiometric coils, the coupling coefficient $k_c$ must also be considered in the calibration. Before the calibration, we calculated $k_c = -0.549$ via a numerical simulation in Opera2D, which was set as a fixed parameter in our model.

For either coil type, the amplitude and phase response was calculated from the time-series of the measured output voltage using the quadrature demodulation technique [24]. Regarding the measurement frequencies, we chose a distribution with many frequencies in the range below $f < 50$ Hz and around the resonance frequency for either coil. Figure 4 exhibits the calibration results for the absolute coil, and figure 5 shows the corresponding data for the gradiometric coil. A striking overall agreement between our models and the measured data is visible. From our measurements, we obtained the values shown in table 1. The standard error of the fitted model for $C_p$ and $L_s$ is 0.2 %.

## 4. Optimized design

For a new, much larger experimental setup with CIFT we needed to design larger induction coil sensors. Naturally, we wanted our sensor to have the largest sensitivity-to-noise ratio possible. In a literature review we could not find an analytical solution for this optimization. Yet, since the inductance and the sensitivity of a coil are related, we can instead maximize the inductance of our sensor design. While the inductance

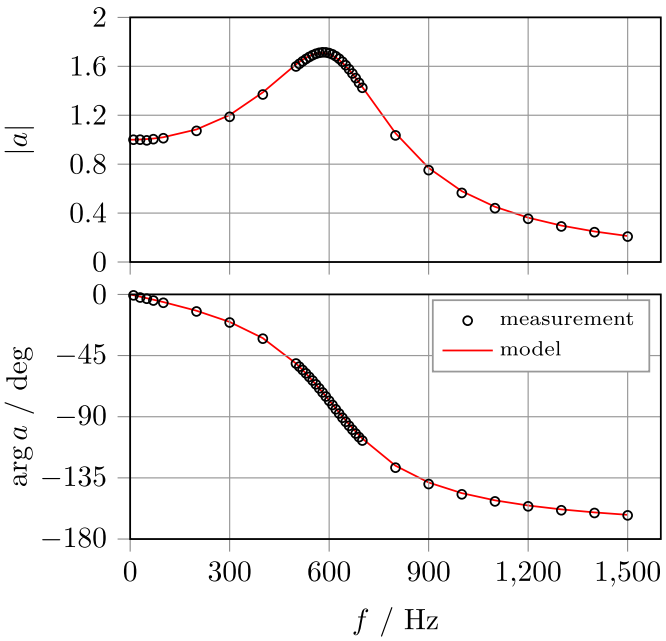


**Figure 5.** Measurement and fitted model for the 2 × 160k gradiometric sensor.

**Table 1.** Results of the calibration of both coils.

| Property | 340k coil | 2 × 160k coil |
|---|---|---|
| Wire diameter | 25 µm | 25 µm |
| Turns | 340 000 | 2 × 160 000 |
| $S$ / V/(T · Hz) | 531.3 | 260.3 |
| $R_s$ / kΩ | 592.0 | 274.9 |
| $L_s$ / H | 463.4 | 71.69 |
| $C_p$ / pF | 412.4 | 505.5 |
| $k_c$ | n./a. | −0.549 |
| $\lvert\underline{a}\rvert$ (3 Hz) − 1 | $5.70 \times 10^{-5}$ | $1.62 \times 10^{-5}$ |
| arg$\underline{a}$ (3 Hz) / deg | $-2.70 \times 10^{-1}$ | $-1.50 \times 10^{-1}$ |

represents a measure for the amount of energy a coil with a driving electrical current can accumulate in its magnetic field, the sensitivity connects an orthogonal magnetic field with the output voltage of the coil. Both quantities have in common that they are only dependent on geometrical parameters, like diameter and number of turns.

A popular empirical approximation for a coil with optimum inductance is the 'four squares design' of Brooks and Turner [25], which is shown in figure 6(a). This design divides the cross section (A-A) of the coil into four connected squares with edge length $c$. The inner two squares represent the cylindrical core, and the outer two contain the turns of wire. The dimensions of the sensor are therefore determined by the edge length $c$ of one of the squares. We could not find designs which yield significantly better inductance for similar compact and easily to manufacture coil shapes.

From this design, Murgatroyd [26, 27] derived two alternatives, which is the three squares design and the five squares design, see figures 6(b) and (c). Both alternatives achieve an inductance about 2 % smaller than that of Brooks'

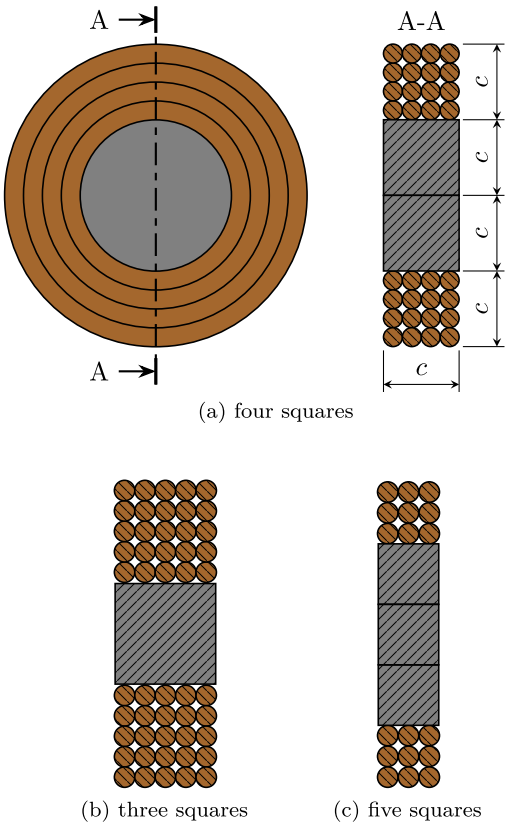


(a) four squares

(b) three squares (c) five squares

**Figure 6.** Construction of induction coil sensors using Brooks' method of squares for constant outer diameter.

design for the same length of wire, which is acceptable for our application.

The coils additionally have to satisfy three following constraints. (A) The maximum allowed coil diameter is 74 mm. This follows from the geometry of the mentioned new experiment, in which the flow structure to be measured extends over 700 mm. In this available space we would like to place up to nine coils, stacked next to each other in the direction of the coils' diameter. If a minimum distance of 3 mm between two adjacent coils is to be kept, the stated coil diameter of 74 mm follows. (B) The coil should be rather flat, which results in choosing the five squares design with $c = 14.8$ mm. The required flatness follows from the magnetic field topology in CIFT experiments. In a very rough approximation, the CIFT secondary magnetic field can be thought of as coming from a single magnetic dipole within the experiment, and then declining outside of the experiment with $r^{-2}$. It then becomes clear that any magnetic field measurement must be conducted as close to the experiment as possible and that a thick coil (with a long cylinder) has the disadvantage that the turns furthest away from the experiment only contribute little to the total output voltage, while still contributing equally to the noise of the sensor. (C) The sensitivity should be larger than $S \geq 530$ V/(T · Hz), which is the same sensitivity the 340k coil exhibits. Since previous CIFT measurements with the 340k coil were successful, we decided the new design should have equal or slightly larger sensitivity.

In order to calculate the performance values for five squares coil design with $c = 14.8$ mm, at first we need equations (2)

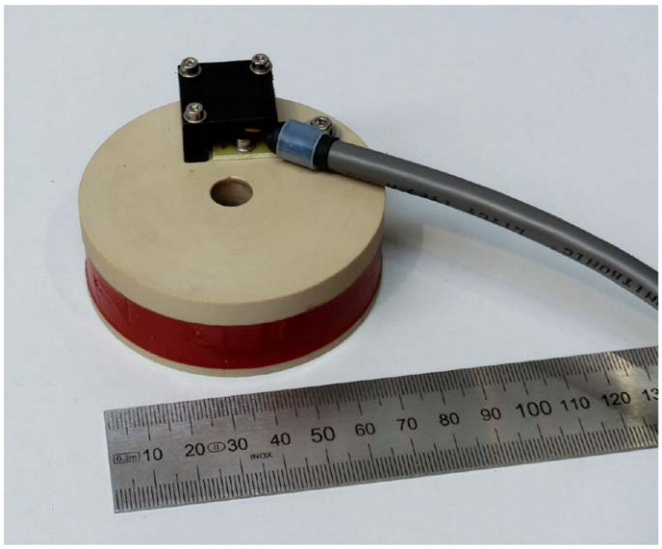

**Figure 7.** New 30k induction coil sensor. The bottom end of the coil would be positioned towards the experiment. The frame is made of PEEK, and the winding is protected with a red rubber coating.

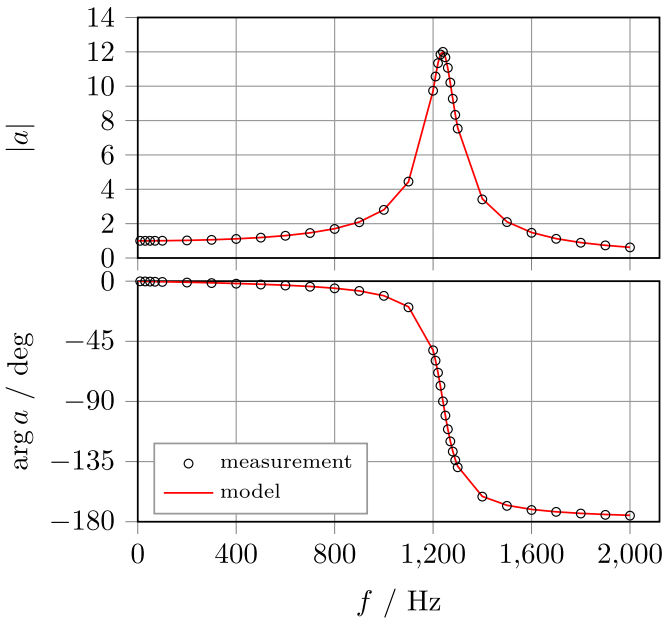


**Figure 8.** Measurement and fitted model for the 30k coil.

for the effective area and (4) for the sensitivity, where $d_i = 3c$ and $d_o = 5c$. For the noise calculations presented in the following sections, we furthermore must calculate the resistance $R$, which can be done in the following manner. First, let us determine the number of turns

$$n = k_f \cdot c^2 \frac{4}{\pi d_c^2}, \tag{19}$$

where $k_f = k_f(d_c)$ is the filling factor of the wire, which describes the ratio between the conducting area and the total area in the square $c^2$ when filled with a wire of core diameter $d_c$. Then we can determine

$$R = n\rho\sqrt{4\pi A}, \tag{20}$$

with $\rho = \rho(d_c)$ being the resistance of the wire per unit length. From the supplier Elektrisola, we selected a wire with $d_w = 71$ µm, $k_f = 0.575$ and $\rho = 4.318$ Ω/m, resulting in the design parameters $n = 31812$, $R = 25.81$ kΩ and $S = 561$ V/(T · Hz). The new sensor was then manufactured by Michael Müller Spulenwickeltechnik.

**Table 2.** Properties of the new 30k coil.

| Property | Value |
|---|---|
| Wire diameter | 71 µm |
| Turns | 32800 |
| $S$/V/(T · Hz) | 577.2 |
| $R_s$/kΩ | 25.03 |
| $L_s$/H | 38.52 |
| $C_p$/pF | 377.6 |
| $\lvert a\rvert$ (3 Hz) − 1 | $5.81 \times 10^{-6}$ |
| arg$a$ (3 Hz) / deg | $-4.68 \times 10^{-2}$ |

The new induction coil sensor, labeled '30k coil', is shown in figure 7. It was calibrated in the same manner as the smaller absolute coil; the results can be seen in figure 8 and table 2. The designed parameters differ only slightly from the actual values of the manufactured sensor.

While the overall agreement of the measured phase and the calculated phase is striking, the model does not agree exactly with the measurement for very low frequencies. We aimed for a phase error of no larger than $1 \times 10^{-2}$ deg, but on average our deviation is $4.4 \times 10^{-2}$ deg. The most probable reason for this is found in small mechanical inaccuracies of our calibration setup. Also, the current sensor we used to measure the excitation current during the calibration might exhibit a small phase shift itself. This will have to be investigated in future work.

## 5. Noise analysis

In the last step, our goal is to quantify the magnetic field noise of our measurement system for all three presented sensors from an analytical approach that is validated by measurements. Knowing the noise spectrum of our sensors enables us to state a maximum measurement uncertainty, and additionally allows us to verify that our optimization was valid.

For the induction coil sensors system, generally three relevant noise sources can be identified [28]. The first one is the thermal noise voltage $u_r$ in a resistor $R$:

$$u_r = \sqrt{4k_b T R \Delta f}. \tag{21}$$

Here, $k_b$ is the Boltzmann constant and $T$ the absolute temperature of the resistor. The variable $\Delta f$ describes the analog bandwidth of the measurement. Since this noise source is independent of $f$, it is called white noise.

Furthermore, we need to consider two current noise sources, which generally create noise voltages by flowing through resistors. The first current noise is the flicker noise $i_f$, which is caused by the non-perfect contact between two conductors while a DC current is flowing through both of them, thereby creating fluctuations in the conductivity:

$$i_f = \sqrt{\frac{K_n I^m \Delta f}{f^n}}. \tag{22}$$

$K_n$ is the flicker noise coefficient, $I$ the DC current, $m$ the flicker noise exponent and $n \simeq 1$. The $1/\sqrt{f^n}$ term makes $i_f$ a pink noise. Lastly, shot noise is created by 'random emission of electrons and by the random passage of charge carriers across potential barriers' [28].

$$i_{\mathrm{sh}} = \sqrt{2qI\Delta f} \tag{23}$$

The quantity $q$ refers to the elementary electric charge.

For all practical matters, we only consider the thermal noise of the sensor itself and the noise of the ADC, since only these two contribute significantly to the total noise, as can be seen in the measurement results at the end of this section. The noise of the ADC is given from its datasheet as SNR = 118 dB when using the $U = 5$ V input. This creates a noise voltage of

$$u_{\mathrm{ADC}} = U \cdot 10^{-\frac{\mathrm{SNR}}{20}} = 6.3\ \mu\mathrm{V}. \tag{24}$$

The noise from the ADC and the coil must be added quadratically to obtain the total noise $u_n$, since they both refer to noise powers:

$$u_n = \sqrt{u_r^2 + u_{\mathrm{ADC}}^2}. \tag{25}$$

It is typically advisable to normalize the measured noise voltage to the bandwidth $\Delta f$ of the measurement. Also, it is often desirable to state the equivalent magnetic field noise $b_n$ rather than the measured noise voltage $u_n$ to facilitate comparing different sensor designs. From these considerations, we can determine the bandwidth-normalized equivalent input noise for our sensors:

$$\frac{b_n}{\sqrt{\Delta f}} = \frac{u_n}{\sqrt{\Delta f}} \cdot \frac{1}{S \cdot f \cdot |\underline{a}(f)|}. \tag{26}$$

Using these equations and the determined values of the equivalent circuit components of the coils, we can analytically calculate $b_n/\sqrt{\Delta f}$ for the coils themselves as well as for the coils with attached ADC, see figure 9.

The shape of the graphs is mainly determined by the amplitude transfer function of the corresponding coils according to equation (26). Consequently the input noise becomes minimal at the resonance frequency. Since the ADC noise was implicitly assumed to be frequency-independent, adding it to the noise of the coil shifts the graphs uniformly towards larger magnetic field noise.

As can be clearly seen, the contribution of the ADC to the total noise is much larger than the contribution of the sensors, especially for the new 30k sensor design. Under no circumstance does the sensor noise exceed 200 pT/$\sqrt{\mathrm{Hz}}$, and the total noise level is always below 1000 pT/$\sqrt{\mathrm{Hz}}$. The new 30k sensor outperforms the smaller two by more than a factor of 5 for a similar sensitivity and exhibits a total noise of no more than 40 pT/$\sqrt{\mathrm{Hz}}$.

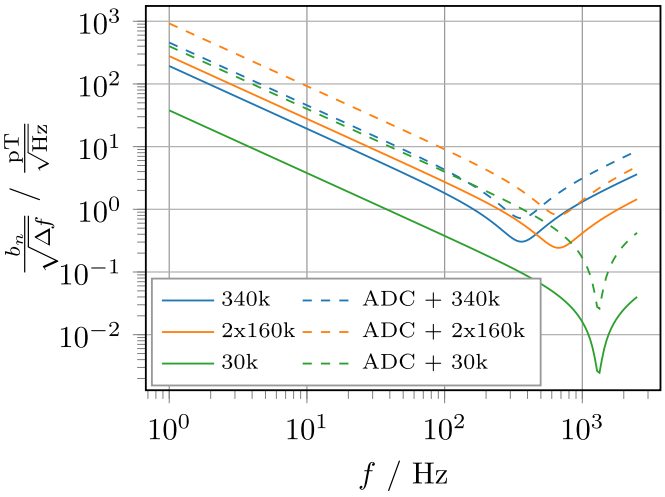


**Figure 9.** Analytical bandwidth-normalized equivalent magnetic field noise of all three induction coils, with and without the ADC.

The total noise never exceeds 1000 pT/$\sqrt{\mathrm{Hz}}$. If a measurement at a center frequency of 1 Hz and a bandwidth of 1 Hz is assumed, we find that with a probability of 99.7 % (corresponding to 3σ) the total precision is better than 5 nT as was stated in the introduction.

The data also reveals that the new optimized 30k sensor does perform about as well as the 340k sensor if the noise of the ADC is included in the calculations. While the optimization of the sensor lead to a significant decrease in its inherent noise, the overall improvement is negligible in the 5 V range. The ADC also features a 250 mV input range with an SNR of only 105 dB, which would decrease the overall noise. The corresponding graphs are not shown because this would exceed the scope of this paper.

In order to validate our theoretical noise analysis, we measured the voltage noise $u_n$ of our magnetic field sensor system for each coil type in the following manner. We placed the sensor into a permalloy box with the inner dimensions of $(90 \times 90 \times 40)\,\mathrm{mm}^3$ and a wall thickness of 1.5 mm. The permalloy box shields the outer magnetic field, so that mostly the sensor noise is measured. With this setup we recorded 100 s of data at a sampling rate of 5 kHz using the default input voltage range of the ADC of 5 V, see figure 10. The recorded time-series was then converted to the frequency domain by means of FFT and scaled with (26) for comparison with the analytical solution. Figure 11 illustrates the procedure.

Figure 12 shows the excellent agreement between the calculations and the measurements. This confirms our theoretical approach and underlines that the dominating performance numbers of induction coils can be specified in the design phase with sufficient accuracy. The peaks in the measured spectra suggest that the permalloy shielding box is too thin for total suppression of the external field, or that the environmental

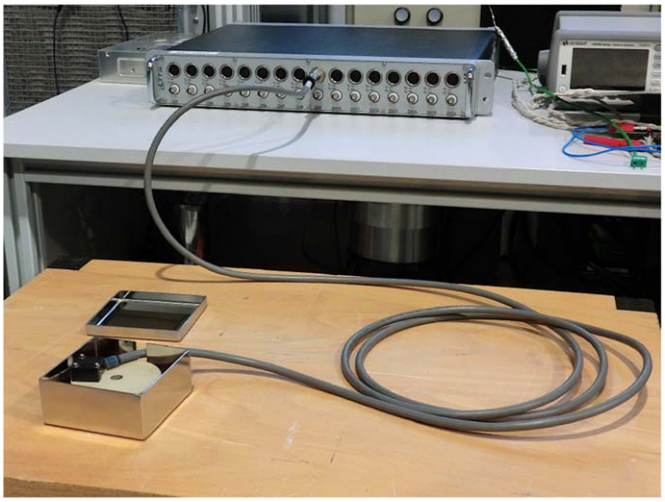

**Figure 10.** Experimental setup for the noise measurement with the lid removed from the mu metal box

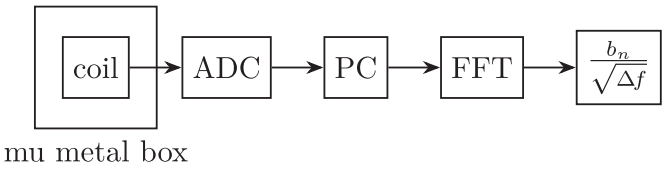


**Figure 11.** Diagram of the noise measurement setup.

magnetic field may enter the box through gaps or the hole for the sensor cable.

For frequencies close to the Nyquist frequency of 2.5 kHz the peaks appear more often because of the logarithmic $f$-axis. Still the lowest part of the measurement graph follows the analytical calculation with good agreement. The sharp decline of the measurement data above 2 kHz as well as the mismatch of the measurement and model around the resonance frequency cannot be explained at the moment.

## 6. Conclusions

In this paper, we demonstrated how absolute and 1st order gradiometric induction coil sensors can be analyzed analytically and by practical experiments. Using their complex-valued transfer functions, the nonlinear amplitude and phase response of these sensor types can be compensated, if the values of their equivalent circuit elements are known. One way to achieve this is by means of a calibration measurement inside a Helmholtz oder Maxwell coil pair.

Furthermore, we designed a new absolute induction coil using the design of five equal squares. This sensor, which will be applied for CIFT measurements, has a total noise of less than 40 $\mathrm{pT}/\sqrt{\mathrm{Hz}}$. In addition, we pointed out how the most important performance numbers of induction coils—such as sensitivity and noise level—can be specified in the design phase by a set of rather simple equations and reliable data sheets.

Future efforts could concern, for example, higher order gradiometric coil sensors and different arrangements of the

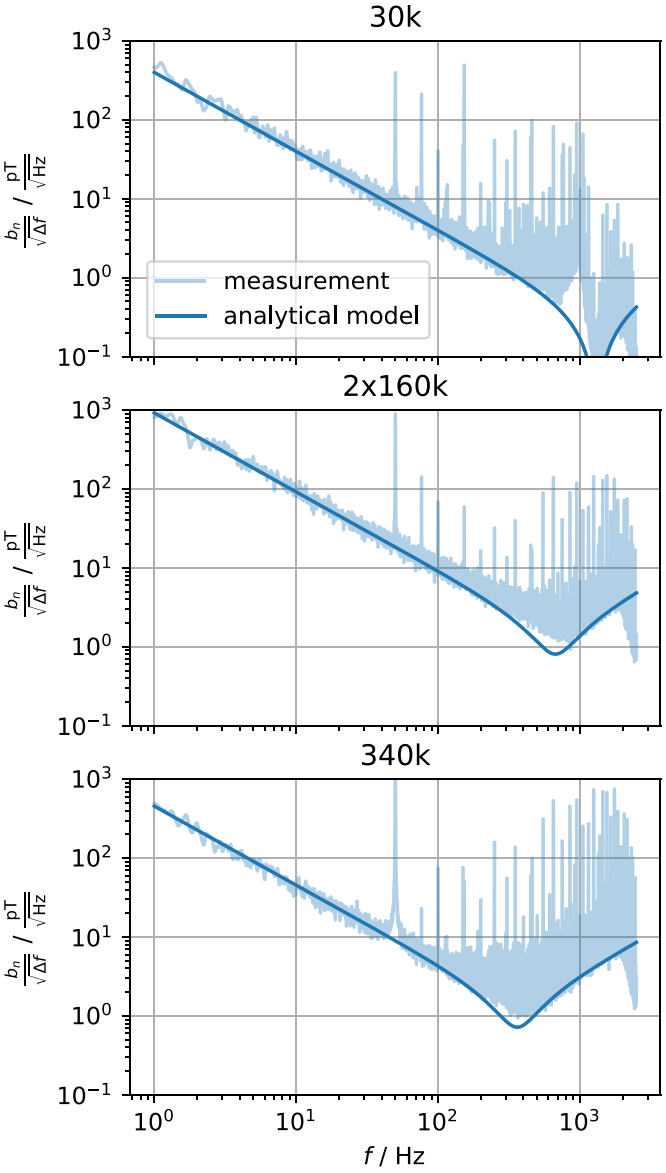


**Figure 12.** Measured equivalent magnetic field noise of all three sensors.

individual windings. Also, compensating the thermal drift of the coils would be of high interest.

## ORCID iD

Matthias Ratajczak https://orcid.org/0000-0003-4320-1921

## References

[1] Stefani F, Gundrum T and Gerbeth G 2004 Contactless inductive flow tomography *Phys. Rev.* E **70** 056306
[2] Wondrak T *et al* 2010 Contactless inductive flow tomography for a model of continuous steel casting *Meas. Sci. Technol.* **21** 045402
[3] Ratajczak M *et al* 2015 Numerical and experimental investigation of the contactless inductive flow tomography

in the presence of strong static magnetic fields *Magnetohydrodynamics* **51** 461–71
[4] Ratajczak M, Wondrak T and Stefani F 2016 A gradiometric version of contactless inductive flow tomography: theory and first applications *Philosophical Trans. Royal Society* A **374** 20150330
[5] NVE Corporation 2005 *AA and AB-series Analog Sensors* 2005 www.nve.com/Downloads/analog_catalog.pdf (Accessed: 30 November 2016)
[6] Jedlicska I, Weiss R and Weigel R 2010 Linearizing the output characteristic of GMR current sensors through hysteresis modeling *IEEE Trans. Ind. Electron.* **57** 1728–34
[7] Bernieri A *et al* 2013 Improving performance of GMR sensors *IEEE Sens. J.* **13** 4513–21
[8] Lara-Castro M *et al* 2017 Portable signal conditioning system of a MEMS magnetic field sensor for industrial applications *Microsyst. Technol.* **23** 215–23
[9] Acevedo-Mijangos J *et al* 2019 Design and fabrication of a microelectromechanical system resonator based on two orthogonal silicon beams with integrated mirror for monitoring in-plane magnetic field *Adv. Mech. Eng.* **11** 168781401985368
[10] Macintyre S A 1999 Magnetic field measurement *The Measurement, Instrumentation, and Sensors Handbook* ed Webster J G (Boca Raton, FL: CRC Press)
[11] Lenz J A review of magnetic sensors *Proc. IEEE* **78** 973–89
[12] Tumanski S 2007 Induction coil sensors—a review *Meas. Sci. Technol.* **18** 31–46
[13] Prance R J, Clark T D and Prance H 2003 Compact room-temperature induction magnetometer with superconducting quantum interference device level field sensitivity *Rev. Sci. Instrum.* 74 3735–9
[14] Grosz A and Paperno E 2012 Analytical optimization of low-frequency search coil magnetometers *IEEE Sens. J.* **12** 2719–23
[15] Prance R J, Clark T D and Prance H 2000 Ultra low noise induction magnetometer for variable temperature operation *Sens. Actuators* B **85** 361–4
[16] Ripka P and Janosek M June 2010 Advances in magnetic field sensors *IEEE Sens. J.* **10** 1108–16
[17] Ripka P (ed) 2001 *Magnetic Sensors and Magnetometers* (Boston, MA: Artech House) 494
[18] Martin Dadić 2013 DC operation analysis of induction coil fluxmeters with integrating amplifiers *Measurement* 46.8 2765–9
[19] Wang X G, Shang X L and Lin J 2016 Development of a low noise induction magnetic sensor using magnetic flux negative feedback in the time domain *Rev. Sci. Instrum.* **87** 054501
[20] Eckert D *et al* 2001 High precision pick-up coils for pulsed field magnetization measurements *Physica B: Condensed Matter* **294** 705–8
[21] Séran H C and Fergeau P 2005 An optimized low-frequency three-axis search coil magnetometer for space research *Rev. Sci. Instrum.* **76** 044502
[22] Macintyre S 1980 A portable low noise low frequency three-axis search coil magnetometer *IEEE Trans. Magn.* **16** 761–3
[23] Luo X *et al* 2014 Research on the comparison testing technique of induction coil sensor *Engineering Technology and Applications* ed F Shao, W Shu and T Tian (Boca Raton, FL: CRC Press) 177–82
[24] Seilmayer M and Ratajczak M 2019 Fundamental principles of spectral methods related to discrete data *Advances in Measurements and Instrumentation: Reviews* ed S Y Yurish (Barcelona: IFSA) vol 1 53–120
[25] Brooks M and Turner H M 1912 Inductance of coils *University of Illinois Bulletin* **910**
[26] Murgatroyd P N 1986 The brooks inductor: a study of optimal solenoid cross-sections *Electric Power Applications, IEE Proc.* B **133** 309–14
[27] Murgatroyd P N 1989 The optimal form for coreless inductors *IEEE Trans. Magn.* **25** 2670–7
[28] Leach M W Jr 1999 Noise measurement *The Measurement, Instrumentation, and Sensors Handbook* ed J G Webster (Boca Raton, FL: CRC Press)